2013

Microstructure and metal-dielectric transition behaviour in a percolative Al2O3-Fe composite via selective reduction

Zidong Zhang
Shandong University, University of Wollongong, zz842@uowmail.edu.au

Runhua Fan
Shandong University

Zhicheng Shi
Shandong University

Kelan Yan
Shandong University

Zhijia Zhang
University of Wollongong, zz755@uowmail.edu.au

See next page for additional authors

Microstructure and metal-dielectric transition behaviour in a percolative Al2O3-Fe composite via selective reduction

Abstract

The electromagnetic (EM) medium plays a key role in many areas, such as communications, stealth technology, etc. Different EM properties are required for different applications. In this paper, we have obtained tunable EM properties in an Al2O3-Fe composite via selective reduction. By adjusting the content of one functional component, the composite shows totally different EM properties, in accordance with the predictions of effective medium theory. Hybrid EM behaviour is obtained near the percolation threshold, which has a close relationship with its microstructure.

Keywords

percolative, metal, behaviour, microstructure, transition, reduction, dielectric, selective, via, composite, fe, al2o3

Disciplines

Engineering | Physical Sciences and Mathematics

Publication Details

Zhang, Z., Fan, R., Shi, Z., Yan, K., Zhang, Z., Wang, X. & Dou, S. (2013). Microstructure and metal-dielectric transition behaviour in a percolative Al2O3-Fe composite via selective reduction. RSC Advances, 3 (48), 26110-26115.

Authors

Zidong Zhang, Runhua Fan, Zhicheng Shi, Kelan Yan, Zhijia Zhang, Xiaolin Wang, and S X. Dou

RSC Advances

RSC Publishing

PAPER

View Article Online
View Journal | View Issue

Cite this: *RSC Adv.*, 2013, **3**, 26110

Microstructure and metal–dielectric transition behaviour in a percolative Al_2O_3–Fe composite *via* selective reduction

Zidong Zhang,[ab] Runhua Fan,*[a] Zhicheng Shi,[a] Kelan Yan,[a] Zhijia Zhang,[b] Xiaolin Wang*[b] and Shixue Dou[b]

Received 20th September 2013
Accepted 22nd October 2013

DOI: 10.1039/c3ra45253k

www.rsc.org/advances

The electromagnetic (EM) medium plays a key role in many areas, such as communications, stealth technology, *etc.* Different EM properties are required for different applications. In this paper, we have obtained tunable EM properties in an Al_2O_3–Fe composite *via* selective reduction. By adjusting the content of one functional component, the composite shows totally different EM properties, in accordance with the predictions of effective medium theory. Hybrid EM behaviour is obtained near the percolation threshold, which has a close relationship with its microstructure.

Introduction

The electromagnetic (EM) medium is becoming increasingly important with the rapid development of technology. Different types can be widely used in many fields, such as wireless communications, stealth technology, *etc.*[1–3] According to the different applications, different EM properties are required.[4,5] For example, in order to optimize the microwave absorption properties of a stealth aircraft's coating, both impedance matching and high energy loss should be taken into consideration. On the contrary, if we want to get good EM wave transparency, which is required in a nose radome, the energy loss should be kept at a relatively low level to maximize the signal.

As is well known, the response of the EM medium to the electromagnetic waves is largely determined by the permittivity (ε) and the permeability (μ).[6,7] For an aircraft's nose radome, in order to maximize the EM waves entering the material, the real and imaginary parts of the complex permittivity and permeability should be comparable, leading to good impedance matching between the material and free space.[8] Otherwise, EM waves will be reflected back at the surface due to the impedance mismatching, which is the basic principle of electromagnetic shielding.[9]

With the development of modern technology, the demand for EM media with different properties has increased dramatically. Moreover, in some special high-technology fields, such as aerospace, electronics, and the military, the EM medium will usually be used in an extreme environment, such as a high-temperature, high-pressure, and corrosive environment. It is impossible for a single material to have different properties to meet the demands of today's industry.[10,11]

Therefore, the electromagnetic composite plays a key role in today's EM field due to its various structural and functional properties, which originate from the components, and their distributions and morphologies, as well as the structure and composition of the interface between the components.[12,13]

In this paper, we report the fabrication of a new kind of EM composite obtained *via* a selective reduction. We use the selective reduction to refine the grains of the metal particles and use Al_2O_3 to control the concentration of free electrons, leading to tunable EM properties in the MHz range. In order to investigate the electromagnetic response of our samples, we use the Bruggeman effective medium theory (EMT) for calculations.[14]

The EM properties of our samples can be well described by the percolation theory and the effective medium theory. Near the percolation threshold, a metal–dielectric hybrid behaviour is obtained in the new EM composite, which has a close relationship to its microstructure and distribution of elements. The fundamentals of tunable EM properties will be discussed based on the experimental results and EMT calculations in this paper.

Experiment

Fe_2O_3/Al_2O_3 mixtures, with different Al_2O_3 molar ratios, were wet-milled in ethanol for 10 hours and dried at 373 K for 3 hours. Then, the powders were pressed under 40 kN for 2 min to prepare plate-shaped samples (15 mm^2 with thickness of 4 mm), followed by pressureless sintering in air at 1573 K for 1.5 hours. The as-sintered products were placed in a tube furnace and isothermally reduced in hydrogen for 3 hours at different temperatures to yield the metal–ceramic composites.

[a]*Key Laboratory for Liquid-Solid Structural Evolution and Processing of Materials (Ministry of Education), Shandong University, Jinan 250061, China. E-mail: fan@sdu.edu.cn; Tel: +86-531-883-93396*

[b]*Institute for Superconducting and Electronic Materials, University of Wollongong, Wollongong, New South Wales 2500, Australia. E-mail: xiaolin@uow.edu.au; Tel: +61-2-4421-5766*

After the reduction process, different types of Fe-rich structures will be formed in the Al_2O_3 matrix with the Al_2O_3 molar ratios changing. For high Al_2O_3 content, island-like Fe-rich structure will be formed in the composite. As the Al_2O_3 content decreases, the Fe-rich island-like structures will be connected together to form a fishnet structure.

The phase identification of samples was performed by X-ray diffraction (XRD) using Cu Kα radiation (λ = 0.15405 nm). Mössbauer (MS) spectra were collected at room temperature, using a ^{57}Co source contained in an Rh matrix. Both the real part and the imaginary part of the permittivity were measured by using an impedance analyzer (Agilent, 4991A) from 10 MHz to 1 GHz.

Phase characterization

According to Todd's research, the reduction reaction of Fe_2O_3 will be affected by the temperature.[15] In this paper, the reduction processes were conducted at 600 °C, 500 °C, and 400 °C by using pure hydrogen. The XRD patterns of the reduced samples (with 50 mol% Al_2O_3) are shown in Fig. 1. The peaks associated with Fe_3O_4, Al_2O_3, and Fe appeared after 3 hours reduction at 600 °C. The phase composition did not change until we decreased the reduction temperature (T_R) to 400 °C. New peaks corresponding to $AlFeO_3$ and $FeAl_2O_4$ appeared, and no peaks of Al_2O_3 could be detected in the sample reduced at 400 °C.

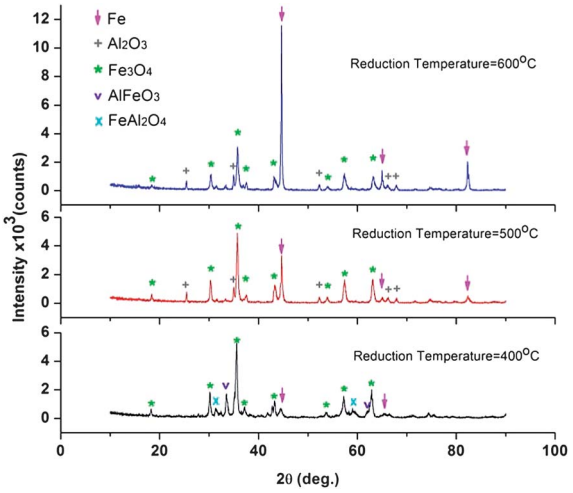

Fig. 1 X-ray diffraction patterns of the samples (50 mol% Al_2O_3) reduced at different temperatures in hydrogen for 3 hours.

Table 1 Parameters of specimens from Mössbauer spectra

Reduction temperature (T_R)	Subspectrum	IS/ mm s^{-1}	QS/ mm s^{-1}	Magnetic field/T	A/%
T_R = 600 °C	Fe^{2+}-doublet	0.96	1.78	—	5.5
	Fe^{3+}-doublet	0.23	0.77	—	6.7
	Fe_3O_4-sextet	0.61	−0.02	42.33	21.1
	Fe_3O_4-sextet	0.33	0.02	46.42	21.9
	Fe-sextet	0.00	0.00	33.07	44.8
T_R = 500 °C	Fe^{2+}-doublet	0.91	1.43	—	11.6
	Fe^{3+}-doublet	0.31	0.82	—	26.8
	Fe_3O_4-sextet	0.31	0.03	47.78	14.5
	Fe_3O_4-sextet	0.65	−0.05	44.14	19.0
	Fe-sextet	0.00	0.00	33.10	28.1
T_R = 400 °C	Fe^{2+}-doublet	0.85	1.27	—	10.4
	Fe^{3+}-doublet	0.26	0.79	—	26.6
	Fe_3O_4-sextet	0.75	0.08	45.06	28.2
	Fe_3O_4-sextet	0.23	−0.09	46.77	26.5
	Fe-sextet	0.00	0.00	33.00	8.3

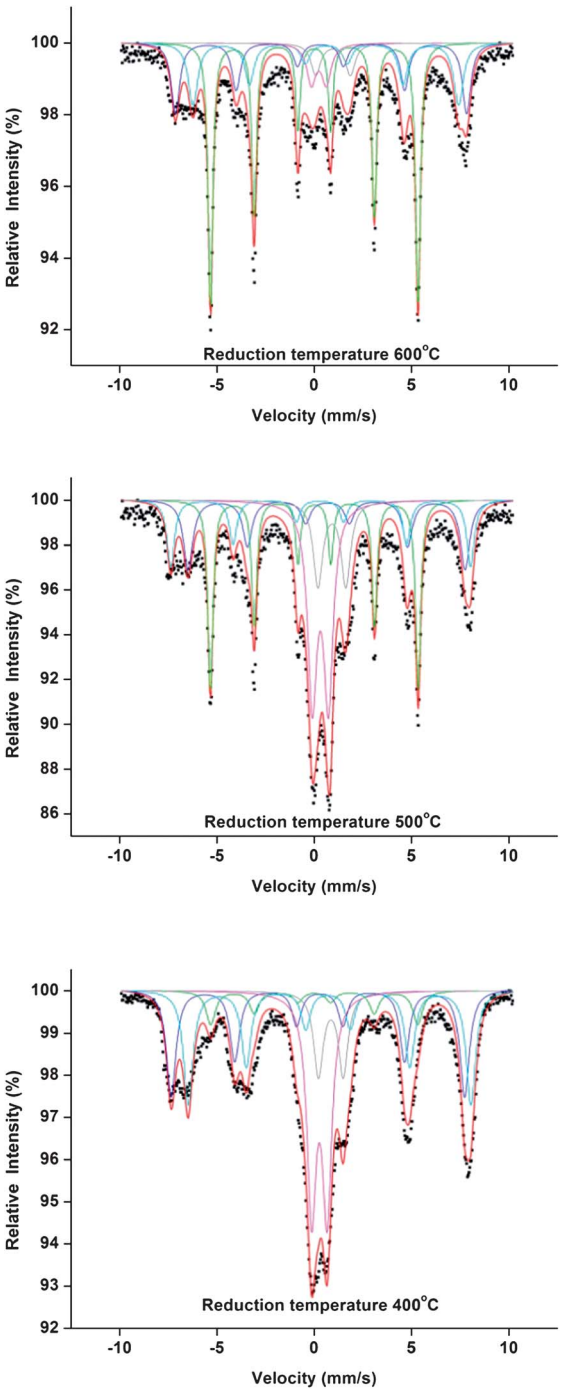

Fig. 2 Mössbauer spectroscopy patterns of the samples (50 mol% Al_2O_3) reduced in hydrogen for 3 hours at different temperatures.

Mössbauer (MS) spectra were collected at room temperature to obtain the accurate phase composition. The Mössbauer spectroscopy parameters are listed in Table 1, while Fig. 2 shows the Mössbauer spectroscopy (MS) pattern of each sample.

As shown in the MS results, all the samples displayed three sextets and two doublets. The sextet with an isomer shift (IS) of 0.00 mm s^{-1}, quadrupole splitting (QS) of 0.00 mm s^{-1}, and magnitude of the hyperfine field of 33 T, can be identified as Fe. Meanwhile, the other two sextets can be associated with Fe_3O_4.[16] The characterization of the doublets becomes a little complex, however, because the ion transfer behaviour has a strong relationship with the reduction temperature. According to Laurent's research, $FeAl_2O_4$ phase will be formed during the reduction reaction of the Fe_2O_3/Al_2O_3 system in H_2 at temperatures lower than 1000 °C.[17] In this case, the doublet with IS of 0.85–0.96 mm s^{-1} and QS of 1.27–1.78 mm s^{-1} represents Fe^{2+} in the $FeAl_2O_4$ spinel structure.[18,19] The other doublet is typical of Fe^{3+} ions substituting for Al^{3+} ions in an alumina lattice.[20]

Electromagnetic results and discussion

The frequency (f) dispersions of the permittivity (ε) are shown in Fig. 3 for the different reduction temperatures. Due to the limitations of the measurement device, however, an effective signal only can be collected from 10 MHz to 1 GHz. As shown in Fig. 3, depending on the reduction temperature, the reduced samples show different EM properties. Based on the results, we can classify the reduced samples into two types.

The first type includes samples reduced at 500 °C and 600 °C. This type shows totally metal-like behaviour in the measurement range. Both the real and the imaginary parts of the permittivity can be well described by the Drude model. [21]

$$\varepsilon(\omega) = 1 - \frac{{\omega_p}^2}{\omega^2 + i\omega_\tau\omega} = \varepsilon' + i\varepsilon''$$

$$\varepsilon'(\omega) = 1 - \frac{{\omega_p}^2}{\omega^2 + {\omega_\tau}^2},\ \varepsilon''(\omega) = \frac{{\omega_p}^2\omega_\tau}{\omega^3 + {\omega_\tau}^2\omega}$$

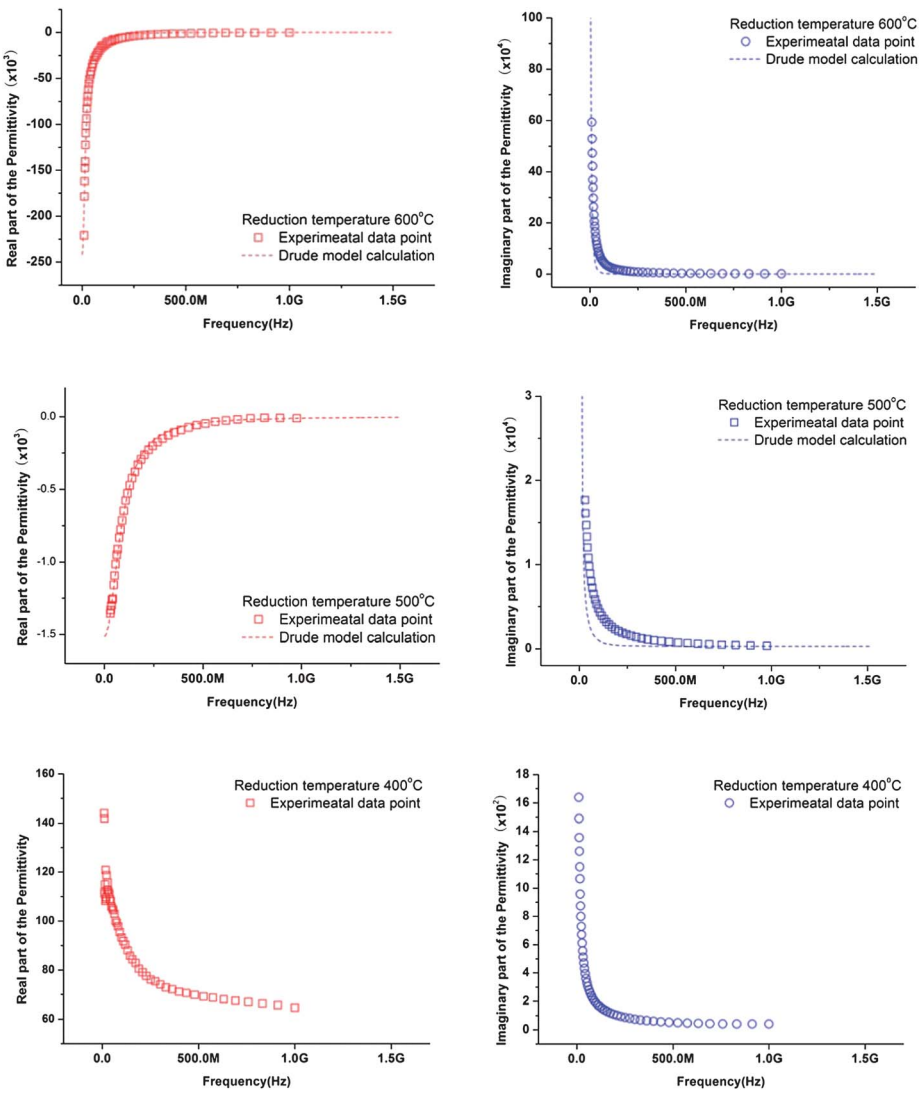

Fig. 3 Permittivity of the samples reduced at different temperatures.

$$\omega_p = \sqrt{\frac{ne^2}{m_{eff}\varepsilon_0}}$$

where, ω_p ($2\pi f_p$) is the plasma frequency, ω is the frequency of the electric field, ω_τ is the damping parameter, ε_0 is the permittivity of vacuum (8.85×10^{-12} F m^{-1}), n is the bulk concentration of carriers, m_{eff} is the electron effective mass, and e is the electron charge (1.6×10^{-19} C).

The concentration of carriers in a metal usually remains on the order of 10^{23}, which places the plasma frequency in the ultraviolet (UV) range (about 10^{15}–10^{17} Hz). In our samples, the electron density is diluted by the non-conductive phase, which contributes to a reduced plasma frequency in the GHz range. The calculated results are also shown in Fig. 3 (dashed lines), which agree well with the experimental data. From the calculation, we can obtain the plasma frequencies of the samples reduced at 600 °C (8.6 GHz) and 500 °C (3.4 GHz). Based on Drude model calculation, we can predict the samples' EM properties. As shown in Fig. 3, the real part of the permittivity take a negative value in the measurement range, which suggest the EM wave will be reflected back in this range and the sample would be transparent to EM waves above the plasma frequency.[13,22]

We consider the sample reduced at 400 °C as typical of the second type, which can be called a metal–dielectric hybrid EM medium. As shown in Fig. 3, when we reduced the reduction temperature to 400 °C, the real part of the permittivity became positive and could not be fitted by the Drude model, as it showed dielectric-like behaviour. Meanwhile, the imaginary part of the permittivity still retained a relatively high value, indicating metal-like behaviour.

According to the effective medium theory (EMT) predictions, the EM properties of metal–dielectric composites will cause them to act as dielectric media for low metal concentrations of less than the percolation threshold and act as dilute metals with an effective permittivity for concentrations beyond the percolation threshold.[23] In our samples, as suggested by the MS results, the final phase composition can be controlled by changing the reduction temperature to obtain different contents of Fe (MS results) in each sample, leading to a different concentration of carriers (n). For the samples reduced at 500 °C and 600 °C (the first type), as the content of conductive phase is beyond the percolation threshold, the medium can be considered as a dilute metal.[24] Interestingly, both metal-like behaviour (large value of ε'') and dielectric-like behaviour (positive value of ε') are obtained in the sample reduced at 400 °C. This kind of EM property, which we have called the 'metal–dielectric hybrid EM property', is not included in the EMT predictions, however.

In order to reach a better understanding of this hybrid EM behaviour, we designed a new experiment to investigate the relationship between the content of conductive phase and the EM properties. Instead of changing the reduction temperature, we changed the content of Al_2O_3 in the Fe_2O_3/Al_2O_3 mixed powder. All the samples were reduced at 600 °C for 3 hours. The frequency (f) dispersions of the permittivity (ε) are shown in Fig. 4. As we can see in Fig. 4, both the real part and the imaginary part show a 'metal to dielectric' transition. As the content of Al_2O_3 is increased (from 40 mol% to 90 mol%), the samples can be divided into two groups on the basis of the real part, a metal-like group (40 mol% to 60 mol% Al_2O_3) and a dielectric-like group (70 mol% to 90 mol% Al_2O_3). Similarly, these two groups are also reflected in the imaginary part (Table 2 and Fig. 4).

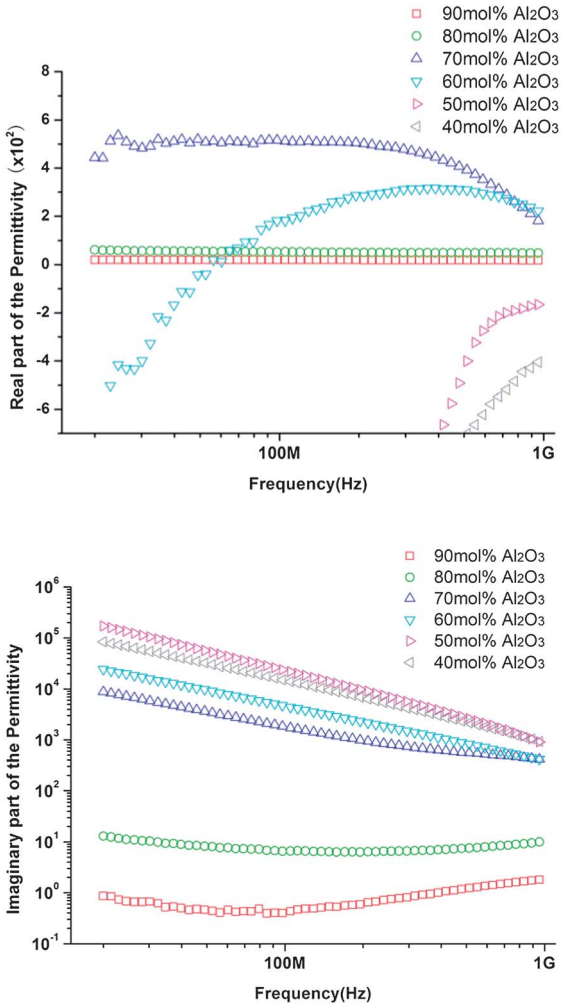

Fig. 4 Frequency dependence of the permittivity for different Al_2O_3 contents.

If we combine the real part with the imaginary part, depending on the Al_2O_3 content, the EM properties can be divided into three types, metal-like behaviour (40 mol%, 50 mol %, and 60 mol%), metal–dielectric hybrid behaviour (70 mol%) and dielectric-like behaviour (80 mol% and 90 mol%). These

Table 2 Metal-like and dielectric-like group

	Metal-like group	Dielectric-like group
ε' (Real part)	40 mol%, 50 mol%, 60 mol%	70 mol%, 80 mol%, 90 mol%
ε'' (Imaginary part)	40 mol%, 50 mol%, 60 mol%,70 mol%	80 mol%, 90 mol%

results clearly show a metal–dielectric transition following the EMT description and strongly suggest that the metal–dielectric hybrid EM property will be obtained near the percolation threshold.

The metal-like behaviour and dielectric-like behaviour can be easily understood according to the EMT, which has already been discussed in our earlier work.[24] The most interesting part is the metal–dielectric hybrid EM property near the percolation threshold. Both EMT and the percolation theory suggest that the EM properties of a percolative composite have a close relationship with the microstructure.[25]

Backscattered electron images and element maps have been collected to find the relationship between the hybrid EM properties and the microstructure. Backscattered electron images and element distributions are shown in Fig. 5. In Fig. 5(a), the Fe-rich areas (red parts) can be considered as conductive paths that form a conductive network, which is spread throughout the whole matrix. Electrons can move freely in this network structure, in almost the same way as in a pure metal. That is the reason for the metal-like behaviour.

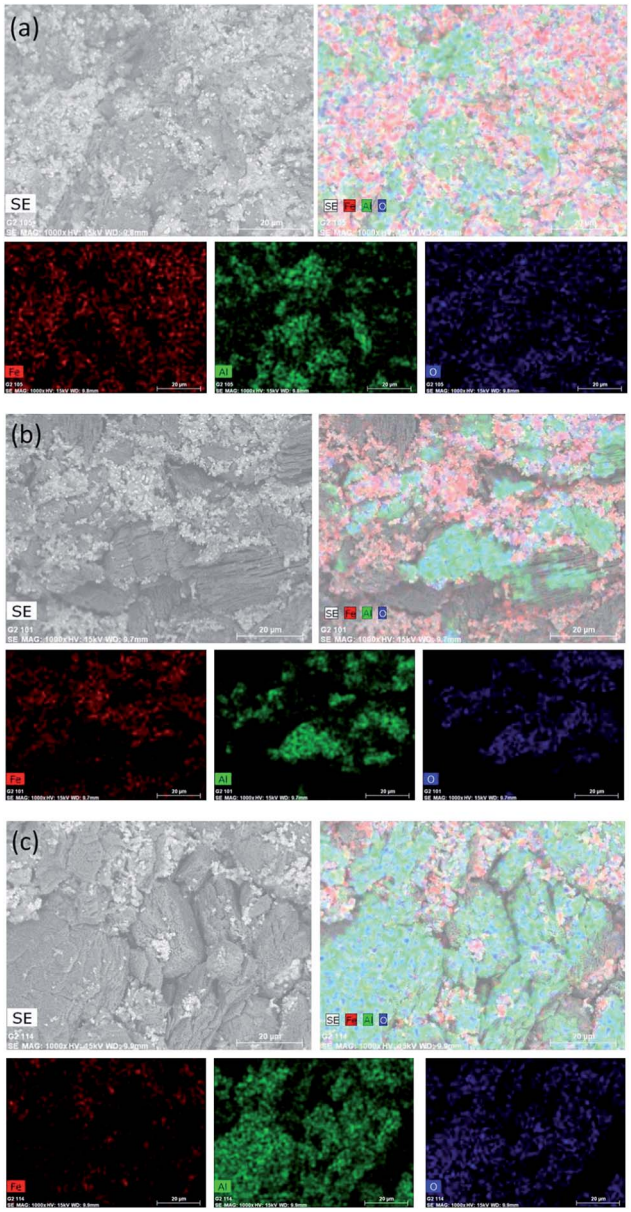

Fig. 5 Backscattered electron images and corresponding element distributions in (a) a metal-like composite (40 mol% Al_2O_3), (b) a metal–dielectric hybrid EM medium (70 mol% Al_2O_3), (c) a dielectric-like composite (80 mol% Al_2O_3).

The whole conductive network will be cut into several local networks as the incorporation of Al_2O_3 is increased to 70 mol%. In this case, a new kind of microcapacitor will be formed in the composite. Each of the microcapacitors is formed by the neighboring local networks and the dielectric layers between them. The large capacitance contributed by each of the microcapacitors can then be correlated with a significant increase in the intensity of the local electric field, leading to a high dielectric constant (large value of the real part of the permittivity). At the same time, current still will be formed in the local network system, leading to a relatively high energy loss. As the mole ratio of Al_2O_3 reaches 80%, the local network will be further divided into island-like structures surrounded by the insulating matrix and the microcapacitor structures will be destroyed, leading to a decrease of the real part of the permittivity. In this case, the free electrons are localized in the matrix and cannot move freely, resulting in a typical dielectric behaviour.

Conclusions

In this paper, percolative composites have been fabricated *via* a selective reduction reaction. The EM properties of the composites can be well described by effective medium theory and percolation theory. Near the percolation threshold, the composite shows an interesting metal–dielectric hybrid EM property, which has a close relationship with its microstructure and element distribution. A local conductive network leading to a large energy loss and a microcapacitor network significantly increases the dielectric constant of the composite.

The authors acknowledge the support of the National Natural Science Foundation of China (51172131), the Program for New Century Excellent Talents in University (NCET-10-518), the Provincial Science and Technology Development Project of Shandong (2007GG10003007, 2007BS04032), the Independent Innovation Foundation of Shandong University (IIFSDU-2010JQ002, GIIFSDU-YYX10011), and the use of facilities within the University of Wollongong Electron Microscopy Centre. The authors thank Dr Tania Silver and Mrs Wenchao Yan for their critical reading of this manuscript, also Mr Xuchuan Wang for his help on the measurements.

Notes and references

1 J. R. Liu, M. Itoh, M. Terada, T. Horikawa and K. Machida, *Appl. Phys. Lett.*, 2007, **91**, 093101.
2 C. Sun and K. N. Sun, *Solid State Commun.*, 2007, **141**, 258.
3 X. G. Liu, D. Y. Geng and Z. D. Zhang, *Appl. Phys. Lett.*, 2008, **92**, 243110.
4 X. Zhang, O. Alloul, J. Zhu, Q. He, Z. Luo, H. A. Colorado, N. Haldolaarachchige, D. P. Young, T. D. Shen, S. Wei and Z. Guo, *RSC Adv.*, 2013, **3**(24), 9453.

5 X. Zhang, Q. He, H. Gu, S. Wei and Z. Guo, *J. Mater. Chem. C*, 2013, **1**(16), 2886.
6 H. Gu, J. Guo, X. Zhang, Q. He, Y. Huang, H. A. Colorado, N. Haldolaarachchige, H. Xin, D. P. Young, S. Wei and Z. Guo, *J. Phys. Chem. C*, 2013, **117**(12), 6426.
7 J. Zhu, X. Zhang, N. Haldolaarachchige, Q. Wang, Z. Luo, J. Ryu, D. P. Young, S. Wei and Z. Guo, *J. Mater. Chem.*, 2012, **22**(11), 4996.
8 Z. D. Zhang, Z. C. Shi, R. H. Fan, M. Gao, J. Y. Guo, X. G. Qi and K. N. Sun, *Mater. Chem. Phys.*, 2011, **130**, 615.
9 D. D. L. Chung, *Carbon*, 2012, **50**, 3342.
10 D. D. L. Chung, Functional Composite Materials, in *Advances in Condensed Matter and Materials Research*, ed. F. Gerard, Nova Science Publ., Hauppauge, NY, 2003, p. 89.
11 D. D. L. Chung, *Mater. Today*, 2002, **5**, 30.
12 H. Gu, Y. Huang, X. Zhang, Q. Wang, J. Zhu, L. Shao, N. Haldolaarachchige, D. P. Young, S. Wei and Z. Guo, *Polymer*, 2012, **53**(3), 801.
13 X. Zhang, S. Wei, N. Haldolaarachchige, H. A. Colorado, Z. Luo, D. P. Young and Z. Guo, *J. Phys. Chem. C*, 2012, **116**(29), 15731.
14 D. A. G. Bruggeman, *Ann. Phys.*, 1935, **416**, 636.
15 A. Mukhopadhyay and R. I. Todd, *J. Eur. Ceram. Soc.*, 2010, **30**, 1359.
16 A. Paesano and C. K. Matsuda, *J. Magn. Magn. Mater.*, 2003, **264**, 264.
17 A. Cordiera, A. Peigneya, E. De Graveb, E. Flahauta and C. Laurent, *J. Eur. Ceram. Soc.*, 2006, **26**, 3099.
18 J. H. Zhu, Z. P. Luo, S. J. Wu, N. Haldolaarachchige, D. P. Young, S. Y. Wei and Z. H. Guo, *J. Mater. Chem.*, 2012, **22**, 835.
19 C. Pecharroman and J. S. Moya, *Adv. Mater.*, 2000, **12**, 294.
20 V. G. de Resende, A. Cordier, E. De Grave, C. Laurent, S. G. Eeckhout, G. Giuli, A. Peigney, G. M. da Costa and R. E. Vandenberghe, *J. Phys. Chem. C*, 2008, **112**, 16256.
21 Z. C. Shi, R. H. Fan, Z. D. Zhang, H. Y. Gong, J. Ouyang, Y. J. Bai, X. H. Zhang and L. W. Yin, *Appl. Phys. Lett.*, 2011, **99**, 032903.
22 C. Kittel, *Introduction to solid state physics*, Wiley, New York, 8th edn, 2004.
23 W. Cai, V. Shalaev, *Optical Metamaterials: Fundamentals and Applications*, Springer Science+Business Media, LLC, USA, 2010.
24 Z.-d. Zhang, R.-h. Fan, Z.-c. Shi, S.-b. Pan, K.-l. Yan, K.-n. Sun, J.-d. Zhang, X.-f. Liu, X. L. Wang and S. X. Dou, *J. Mater. Chem. C*, 2013, **1**, 79.
25 C. W. Nan, Y. Shen and J. Ma, *Annu. Rev. Mater. Res.*, 2010, **40**, 131.